An Internally Staged Hollow-Fiber Permeator for Gas Separation

Conventional membrane permeation of gases employ a one-step process between the feed and the product on two sides of a membrane. By applying the overall driving force change through a two-step process using two membranes in one device, we illustrate theoretically the possibility of achieving a much higher enrichment without any extra energy consumption. Such an internally staged permeation is experimentally carried out in a hollow-fiber permeator with two sets of asymmetric cellulose acetate hollow fibers for the systems of O_2—N_2 (air) and CO_2—N_2. The superior enriching performance of the internally staged permeator over the same permeator operated in the conventional mode is demonstrated experimentally. A cocurrent flow pattern is found to be superior to a countercurrent flow pattern for the conditions employed. The simulation model incorporating fiber lumen pressure drop predicts the experimental performance quite well. A further improvement in performance can be achieved by recycling the intermediate pressure shell reject stream to the feed stream. The energy requirement in an internally staged permeator without recycle is less than that of a conventional permeator with permeate recycle.

M. Sidhoum
S. Majumdar
K. K. Sirkar
Center for Membranes
and Separation Technologies
Department of Chemistry
and Chemical Engineering
Stevens Institute of Technology
Hoboken, NJ 07030

Introduction

Gas separation by permeation through nonporous polymeric membranes in hollow-fiber or spiral-wound form is now widely practiced in industry. Such a separation is carried out by imposing a large pressure difference across the membrane; permeate emerging from the membrane at a low pressure is enriched in the fast gas. However, the extent of enrichment is often not high enough. Considerable research is therefore underway to develop either improved membranes or better separation schemes.

Suppose that the large pressure difference between the feed gas and permeate gas is implemented in two permeation steps with two membranes; the permeate emerging from the first membrane in the first step at an intermediate pressure, is imposed on the second membrane for the second permeation step, Figure 1. Would this two-step gas permeation process yield a richer permeate than a single-step gas permeation process if the feed and the final permeate pressures were maintained the same in both cases? We answer this question first by making calculations with membranes of differential area, thus avoiding the complications of a regular stage analysis.

What are the implications if the two-step gas permeation process turns out to be more efficient than the conventional one-step gas permeation process? Could one implement such a concept in one permeator using either hollow-fiber or flat membranes? We explore this idea by fabricating a hollow-fiber permeator with two sets of fibers, one set for each permeation step. At every axial location in the permeator, the permeate from the first membrane is the feed for the second membrane, Figure 2. Thus, the two-step permeation process is locally coupled. A question of considerable interest is whether, other conditions remaining constant, this permeator will perform better separation than a conventional one-step hollow-fiber permeator. To answer this question, we provide here experimental data for two systems, O_2—N_2 (air) and CO_2—N_2.

Permeators with two sets of hollow fibers are not entirely novel. Such permeators containing two completely different kinds of hollow fibers, cellulose acetate and silicone, have been studied experimentally by Ohno et al. (1977), Perrin and Stern (1986), and Sengupta and Sirkar (1987, 1988). In these permeators, the two different fibers are exposed to the same feed gas introduced through the shell side. Binary gas mixture separation in such a

Correspondence concerning this paper should be addressed to K. K. Sirkar. M. Sidhoum is currently with Institut Algerien Du Petrole, Boumerdes, Algeria.

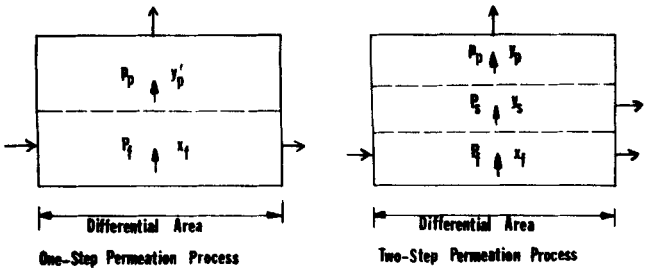

Figure 1. One-step and two-step permeation processes.

permeator has been modeled by Ohno et al. (1977) and Perrin and Stern (1985). Ternary gas mixture separation in such permeators has been modeled by Sirkar (1980) and Sengupta and Sirkar (1984, 1987). However, an experimental study of a dual fiber permeator for a two-step gas permeation is totally novel. Only a few preliminary theoretical calculations under idealized conditions are available (Sidhoum et al., 1988b).

In a conventional one-step hollow-fiber permeator, permeate composition varies significantly along the permeator length. The higher the stage cut, the larger is this variation. In a conventional two-stage permeation process, permeates of differing composition in the first stage get mixed together and fed into the second stage, Figure 3. How does the permeate from the second stage of this conventional two-stage process compare with the process permeate from a hollow-fiber permeator with a two-step permeation having the same total membrane area? We have explored this aspect by using generally accepted models of conventional hollow-fiber permeators.

Achievement of a two-step permeation process with two sets of hollow fibers in a permeator appears possible only if the first permeation step is carried out with a tube-side feed, since concentric hollow fibers are unrealistic. Recent experimental studies by Sidhoum et al. (1988a, 1988b) have demonstrated that excellent separation is obtained with high-pressure feed in the lumen of asymmetric cellulose acetate (CA) hollow fibers with the skin on the outside surface. In our permeator with two sets of fibers for two-step permeation, the high-pressure feed gas is therefore introduced to the lumen of the first set of fibers, Figure 2. The shell side is maintained at a pressure between that of the feed gas and the low final process permeate pressure in the lumen of the second set of fibers. We can describe this two-step permeation process as internally staged permeation and the two-

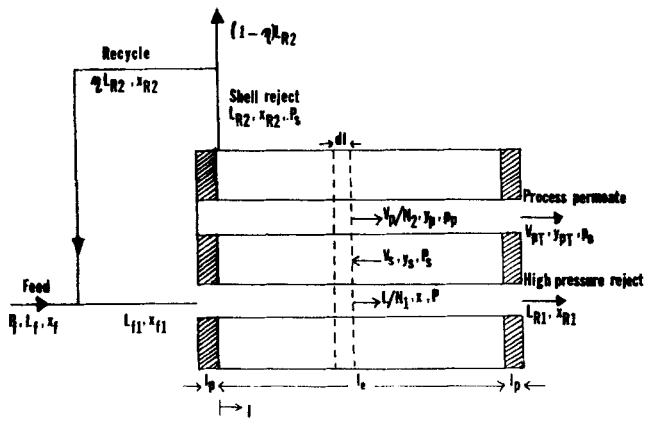

Figure 2. ISP in countercurrent mode with recycle.

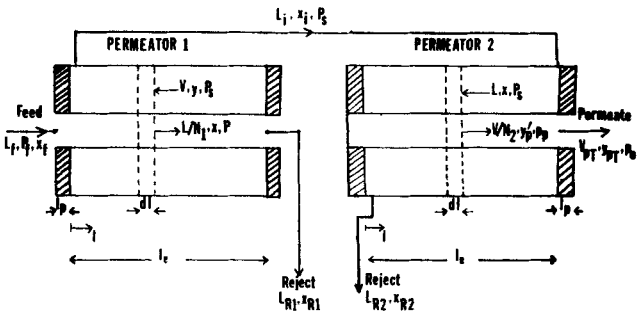

Figure 3. Two-stage cascade configuration: countercurrent flow pattern.

fiber permeator for this objective as an internally staged permeator (ISP).

In this paper, we describe the operation of a hollow-fiber based ISP and compare the experimental results with a model that incorporates fiber lumen pressure drop for both cocurrent and countercurrent flow. We compare its experimental performances with those of the same two-fiber permeator operated as a conventional single-stage permeator. The membranes used in the permeator are asymmetric CA hollow fibers with the dense skin on the outside surface. We evaluate the performance of the locally coupled two-step permeation in one permeator in comparison with that of a conventioanl two-stage, two-permeator configuration, Figure 3. Further, we theoretically explore how the recycle of the intermediate pressure permeate from the shell side of an ISP to the feed gas can significantly enhance the final process permeate quantity and quality without undue penalty in energy cost. Finally, we compare the energy requirement in a conventional permeator having partial permeate recycle with that in an ISP without any recycle.

Internally Staged Permeation Model

We develop mathematical descriptions of a two-step permeation process under two categories: zero stage cut permeation, and an ISP with two sets of hollow fibers with or without recycle.

Zero stage cut permeation

Consider the two-step permeation process in Figure 1, which shows two membranes of differential area. Membrane I is subjected to a binary feed of composition x_f and pressure P_f. The other side of this membrane is at a pressure $P_s < P_f$. Let the permeate composition emerging from membrane I be y_s. We assume that simple cross-flow equations (Walawender and Stern, 1972; Pan and Habgood, 1974) can be used for this pointwise permeation calculation. Then

$$y_s = \frac{\alpha(x_f - \gamma_s y_s)}{\alpha(x_f - \gamma_s y_s) + (1 - x_f) - \gamma_s(1 - y_s)} \tag{1a}$$

where

$$\alpha = Q_1/Q_2 \quad \text{for homogeneous membrane}$$
$$= (Q/d)_1/(Q/d)_2 \quad \text{for asymmetric membrane}$$

and

$$\gamma_s = P_s/P_f \tag{1b}$$

The quadratic in Eq. 1a has the following solution:

$$y_s = \frac{1 + (\alpha - 1)(x_f + \gamma_s) - \{[1 + (\alpha - 1)(x_f + \gamma_s)]^2 - 4\alpha(\alpha - 1)\gamma_s x_f\}^{1/2}}{2(\alpha - 1)\gamma_s} \tag{2}$$

This permeate from the membrane I is now imposed as feed on membrane II. We assume that:

1. The permeabilities and the ideal separation factor for species 1 and 2 through membrane II are identical to those of membrane I
2. Cross-flow equations are valid for permeation through membrane II into the final permeate region at pressure p_p
3. Permeabilities through membrane II are unaffected by the pressure levels

Assumptions 1 and 3 are supported by pure-component permeability data provided later in the paper. For zero stage cut permeation, cross-flow equations are obviously valid, justifying assumption 2. In fact, countercurrent, cocurrent, and cross-flow models are identical in the limit of zero stage cut permeation. Then, for simple cross-flow permeation from the intermediate pressure P_s to final permeate pressure p_p, the equation for final permeate mole fraction y_p can be written as

$$y_p = \frac{\alpha(y_s - \gamma_p y_p)}{\alpha(y_s - \gamma_p y_p) + (1 - y_s) - \gamma_p(1 - y_p)} \tag{3a}$$

where

$$\gamma_p = p_p/P_s \tag{3b}$$

The solution of this quadratic is

$$y_p = \frac{1 + (\alpha - 1)(y_s + \gamma_p) - \{[1 + (\alpha - 1)(y_s + \gamma_p)]^2 - 4\alpha(\alpha - 1)\gamma_p y_s\}^{1/2}}{2(\alpha - 1)\gamma_p} \tag{4}$$

The values of y_p and y_s thus obtained for given x_f, P_f, P_s, and p_p are valid only at a point in cross flow. Effectively this implies zero stage cut for the stage with feed composition x_f as well as for the intermediate stage with feed composition y_s. The final permeate composition y_p from this two-step permeation should be compared with that from a conventional one-step permeation, also shown in Figure 1, subject to a feed x_f at P_f and a permeate at pressure p_p:

$$y'_p = \frac{\alpha(x_f - \gamma' y'_p)}{\alpha(x_f - \gamma' y'_p) + (1 - x_f) - \gamma'(1 - y'_p)} \tag{5a}$$

where

$$\gamma' = p_p/P_f \tag{5b}$$

Note that there are two limiting situations for zero stage cut permeation:

1. $P_s = P_f \rightarrow \gamma_s = 1$
2. $P_s = p_p \rightarrow \gamma_s = \gamma'$

In these two limits, the two-step permeation becomes identical to one-step permeation. Therefore, the y_p value for both limits should be equal to y'_p.

An internally staged hollow-fiber permeator with or without recycle

A. Countercurrent Flow. Figure 2 shows one fiber acting as membrane I and another fiber acting as membrane II. Both fibers have the dense skin on the outside surface. High-pressure feed gas at a pressure P_f enters the lumen of membrane I. The permeate from this fiber comes to the shell side maintained at a pressure P_s ($<P_f$). The permeate in the shell side flows countercurrent to the high-pressure feed gas and exits through a shell outlet. The shell-side gas is exposed everywhere to the dense skin of the second hollow fiber (membrane II), whose lumen is at a pressure lower than P_s. A fraction of the shell-side gas permeates through membrane II; this process permeate flows countercurrent to the shell-side gas and exits at a pressure of p_o. Along the potted length l_p at both ends, there is no permeation.

Although we have shown only one fiber for each permeation step, in reality there will be thousands of fibers for each step. The present model has N_1 fibers for the first permeation step and N_2 fibers for the second. The following assumptions were used to develop the model equations for countercurrent flow in this ISP:

1. The asymmetric CA membrane can be modeled as a homogeneous membrane regardless of whether we have tube-side feed or shell-side feed (Sidhoum et al., 1988a).
2. The specific permeability $(Q/d)_i$ of any species i is independent of pressure and composition (Sidhoum et al., 1988a).
3. There is no axial mixing of gases in the shell side along the permeator length. However, there is no radial concentration profile in the shell space of the permeator. The same assumptions are valid in the fiber lumen also. Shell-side pressure is constant everywhere.
4. Fiber lumen pressure drop can be obtained assuming Poiseuille flow.
5. CA hollow fibers are not deformed by pressurization from the outside or the inside (Sengupta and Sirkar, 1987; Sidhoum et al., 1988a).
6. There is no concentration polarization in the porous substrate of membrane I exposed to feed gas in the lumen (Sidhoum et al., 1988a).

Assumption 3—a lack of axial mixing in the shell side—presupposes a long permeator with a well-packed fiber bundle. Axial mixing effects are, in general, minor (Kao et al., 1987).

Figure 2 shows that a fraction η of the shell-side reject stream at an intermediate pressure P_s is recycled to the fresh feed stream of composition x_f; thus the feed actually entering the lumen of hollow-fiber membrane I has a composition x_{f1} ($>x_f$). The equations given below are valid for partial recycle of the intermediate pressure stream to the feed. Most of this paper is concerned with a situation where $\eta = 0$, the results for which are obtained simply by putting $\eta = 0$ in these equations.

Overall and component material balances at permeator inlet

$$L^*_{f1} = 1 + \eta L^*_{R2} \tag{6}$$

$$x_{f1} = (x_f + \eta L^*_{R2} x_{R2})/L^*_{f1} \tag{7a}$$

where

$$L_{f1}^* = L_{f1}/L_f; \qquad L_{R2}^* = L_{R2}/L_f \tag{7b}$$

Permeation equations

$$dx/dl^* = -K_1^I\{\alpha(1-x)(\gamma x - \gamma_s y_s) - x[\gamma(1-x) - \gamma_s(1-y_s)]\}/L^* \tag{8}$$

$$dy_s/dl^* = -K_1^I\{\alpha(1-y_s)(\gamma x - \gamma_s y_s) - y_s[\gamma(1-x) - \gamma_s(1-y_s)]\}/V_s^* + K_1^{II}\{\alpha(1-y_s)(y_s - \gamma_p y_p) - y_s[1 - y_s - \gamma_p(1-y_p)]\}/V_s^* \tag{9}$$

$$dy_p/dl^* = K_1^{II}\{\alpha(1-y_p)(y_s - \gamma_p y_p) - y_p[1 - y_s - \gamma_p(1-y_p)]\}/V_p^* \tag{10}$$

$$dL^*/dl^* = -K_1^I[\alpha(\gamma x - \gamma_s y_s) + \gamma(1-x) - \gamma_s(1-y_s)] \tag{11}$$

$$dV_s^*/dl^* = -K_1^I[\alpha(\gamma x - \gamma_s y_s) + \gamma(1-x) - \gamma_s(1-y_s)] + K_1^{II}[\alpha(y_s - \gamma_p y_p) + 1 - y_s - \gamma_p(1-y_p)] \tag{12}$$

$$dV_p^*/dl^* = K_1^{II}[\alpha(y_s - \gamma_p y_p) + 1 - y_s - \gamma_p(1-y_p)] \tag{13}$$

where

$$\gamma = P/P_f;\ \gamma_s = P_s/P_f;\ \gamma_p = p_p/P_s$$
$$V_s^* = V_s/L_f;\ V_p^* = V_p/L_f;\ L^* = L/L_f$$
$$l^* = l/l_e;\ \alpha = (Q/d)_1/(Q/d)_2$$
$$K_1^I = \pi D_{lm} N_1 (Q/d)_2 l_e P_f/L_f$$
$$K_1^{II} = \pi D_{lm} N_2 (Q/d)_2 l_e P_s/L_f$$
$$D_{lm} = (D_o - D_i)/\ln(D_o/D_i) \tag{14}$$

Pressure drop equations

$$d\gamma/dl^* = -K_2^I L^*/\gamma \tag{15}$$

$$d\gamma_p/dl^* = -K_2^{II} V_p^*/\gamma_p \tag{16}$$

where

$$K_2^I = 128\,\mu\, R_g T l_e L_f/(\pi D_i^4 N_1 P_f^2)$$
$$K_2^{II} = 128\,\mu\, R_g T l_e L_f/(\pi D_i^4 N_2 P_s^2) \tag{17}$$

Since there is no permeation through the potted length of the fibers at the permeator ends, integration of Eqs. 15 and 16 will provide the appropriate boundary conditions of γ at the inlet of the active fiber length (at $l^* = 0$) and γ_p at the end of the active fiber length (at $l^* = 1$):

at $l^* = 0$, $V_p^* = 0$; $L^* = L_{f1}^*$; $x = x_{f1}$; $\gamma = [1 - 2K_2^I L_{f1}^* (l_p/l_e)]^{1/2}$

$$y_p = \frac{1 + (\alpha-1)(x_{R2} + \gamma_p) - \{[1 + (\alpha-1)(x_{R2} + \gamma_p)]^2 - 4\alpha(\alpha-1)\gamma_p x_{R2}\}^{1/2}}{2(\alpha-1)\gamma_p} \tag{18}$$

at $l^* = 1$, $V_s^* = 0$; $\gamma_p = [\gamma_0^2 + 2K_2^{II} V_{pT}^* (l_p/l_e)]^{1/2}$

$$y_s = \frac{\gamma_1 + (\alpha-1)(\gamma_1 x_{R1} + \gamma_s) - \{[\gamma_1 + (\alpha-1)(\gamma_1 x_{R1} + \gamma_s)]^2 - 4\alpha(\alpha-1)\gamma_1\gamma_s x_{R1}\}^{1/2}}{2(\alpha-1)\gamma_s} \tag{19}$$

Note that $\gamma_o = p_o/P_s$ is specified by the permeate exit pressure p_o. Note further that the derivatives in Eqs. 9 and 10 are indeterminate at $l^* = 1$ (where $V_s^* = 0$) and at $l^* = 0$ (where $V_p^* = 0$), respectively. The indeterminacies can be removed by applying L'Hospital's rule to both expressions. For example,

$$\left.\frac{dy_p}{dl^*}\right|_{l^*=0} = \frac{[\alpha(1-y_p) + y_p]\left.\dfrac{dy_s}{dl^*}\right|_{l^*=0}}{2y_s(\alpha-1) - 3\gamma_p y_p(\alpha-1) + \gamma_p(\alpha-2) + 2} \tag{20}$$

A similar effort for (dy_s/dl^*) at $l^* = 0$ leads to a much larger expression, which is available in a thesis by Sidhoum (1988).

B. Cocurrent Flow. The analysis for the cocurrent flow pattern, Figure 4, is similar to that of the countercurrent flow pattern. The differential equations for L^*, x, γ, and γ_p are identical to the equations for the countercurrent flow pattern. The derivative expressions of V_s^* and y_s are also similar to the countercurrent mode, except that the signs are reversed. For cocurrent flow, V_p^* and y_p are obtained from simple material balance equations. For details, the reader is referred to the thesis by Sidhoum (1988) and a paper by Sidhoum et al. (1988b).

Experimental Equipment and Procedure

The CA hollow fibers of unknown degree of acetylation were obtained from a DOW reverse osmosis module (Module No. 96-05, Permutit Co., Paramus, NJ). These fibers were made suitable for gas separation by Sengupta (1985) using the solvent-exchange and drying technique recommended by MacDonald

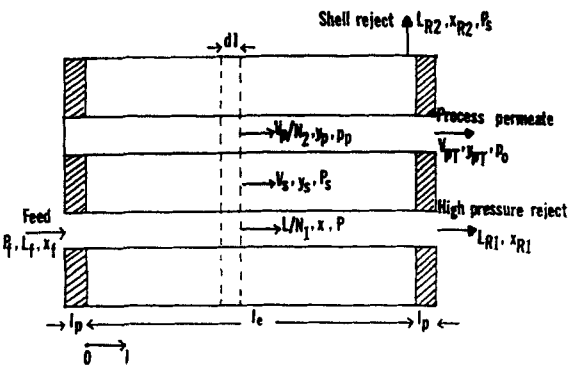

Figure 4. ISP in cocurrent flow pattern.

and Pan (1974). The dried fibers used here come from the same bundle used by Sengupta and Sirkar (1987) and Sidhoum et al. (1988a, b).

A high fiber packing density is needed in an ISP to minimize any axial diffusional effects and channeling. A tight bundle of two sets of CA hollow fibers were therefore housed in a 0.32 cm Teflon pipe of 0.61 cm ID and 1.03 cm OD (Cole-Parmer, Chicago, IL). This Teflon pipe was first inserted into a 1.27 cm schedule 40 SS pipe. The concentric annular space between the Teflon pipe and the SS pipe was filled with an epoxy resin. Each end of the SS pipe was connected to the straight end of a 1.27 cm SS 45° lateral connection whose two branch openings were used for one end of each set of fibers, as shown in Figure 5. To each such branch opening a hex nipple was attached for fiber potting with epoxy.

A total of 150 fibers, with 100 fibers in first set (N_1) and 50 fibers in the second set (N_2), were intimately mixed together to prepare a fiber bundle. However, the two sets of fibers were separated at both ends of the bundle. The details of bundle insertion in the permeator shell and the fiber potting procedure are given in Sidhoum (1988). The epoxy used for potting was a C4 resin with activator D in the ratio of 4:1 by weight (Beacon Chemical Co., Mt. Vernon, NY). The geometrical characteristics of the permeator are given in Table 1.

The experimental apparatus shown schematically in Figure 6 comprised the following lines connected to the ISP: feed, high-pressure reject, shell reject, and process permeate gas lines. The ISP module was immersed in a constant 25°C water bath. The instrumentation in the high-pressure feed and the high-pressure reject lines was essentially similar to that used in the feed-inside (tube-side feed) mode of operation by Sidhoum et al. (1988a), with the high-pressure feed entering the fiber lumen. The process permeate gas line was similar to the permeate line of the setup mentioned in the same reference. The shell reject line consisted of an electronic flow transducer (Matheson), a pressure gauge, and a backpressure regulator (Fairchild Co., Salem, NC).

Using two four-way switching valves (Whitey Co., Highland Heights, OH), any gas sample was directed to a Varian Model 3400 gas chromatograph (GC) when needed. The gas sample could be either high-pressure reject, shell reject, or the process permeate stream. The GC was used with a thermal conductivity detector and a CTR column (Sengupta and Sirkar, 1987; Sidhoum et al., 1988a). The column was calibrated using standard gravimetric gas mixtures as well as gas mixtures of known compositions prepared by using a Modular Dyna Blender (Matheson, model 8250). Each gas stream, when not being analyzed, was vented to atmosphere or sent to a bubble flow meter.

Table 1. Geometrical Characteristics of Internally Staged Permeator

No. of fibers in first stage	100
No. of fibers in second stage	50
Total no. of fibers	150
Fiber OD, cm	2.30×10^{-2}
Fiber ID, cm	0.84×10^{-2}
Potted length, cm	6.2
Permeation area in first stage, cm^2	239.5
Permeation area in second stage, cm^2	119.6
Total permeation area, cm^2	359.1
Teflon pipe OD, cm	1.03
Teflon pipe ID, cm	0.61
Packing fraction	0.21

The pure-component permeabilities of the first set of fibers were measured *in situ* in the tube-side feed mode. In this case the two end openings of the second set of fibers were plugged. The high-pressure reject line was also kept closed. The first set of fibers was internally pressurized and, at steady state, the total permeation rate collected from the shell reject line was measured. The feed inlet and closed end fiber pressures were also recorded.

The pure-component permeabilities of the second set of fibers were measured *in situ* in the shell-side feed mode where the shell reject line was kept closed. The pure-component feed gas at a given pressure was introduced through the second shell opening. Again, feed pressure and permeate rate collected from the process permeate line were measured at steady state. Both ends of the first set of fibers were plugged during this experiment.

To start binary separation runs, the following procedure was adopted. The pressurization of the ISP proceeded carefully to prevent any accidental failure of the first set of fibers. As the feed gas flow rate was gradually increased, the inlet feed gas pressure and the shell-side pressure were increased. At steady state, all flow rates, compositions, and pressures in the different gas lines were measured. At a given feed inlet pressure, different stage cuts and gas stream compositions were achieved by varying the feed flow rate.

Results and Discussion

We consider the results of internally staged permeation under several categories. First, the results of theoretical calculations of

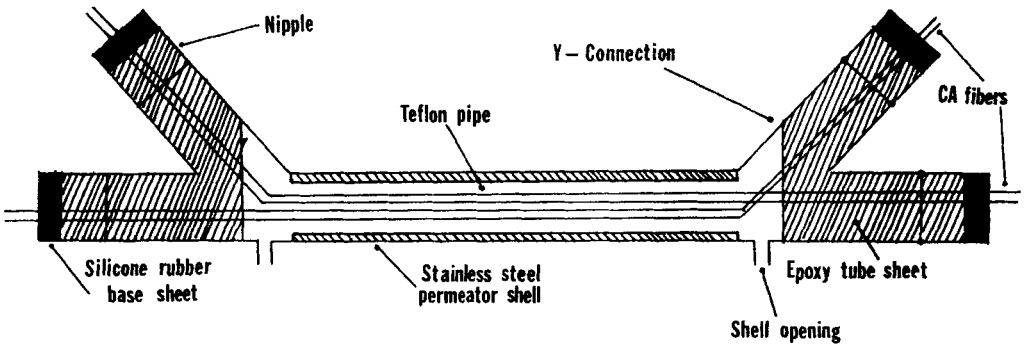

Figure 5. Fiber and potting arrangements in ISP.

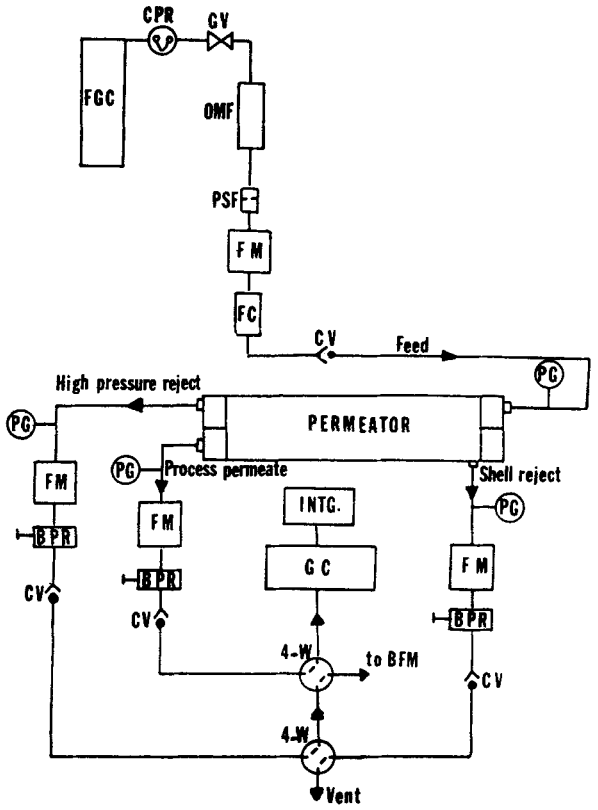

Figure 6. Experimental apparatus.

BPR, back-pressure regulator
BFM, bubble flow meter
CPR, cylinder pressure regulator
CV, check valve
FC, flow controller
FGC, feed gas cylinder
FM, flow meter
GC, gas chromatograph
GV, gate valve
INTG, integrator
OMF, oil and moisture filter
PG, pressure gauge
PSF, particulate solids filter
4-W, four-way valve

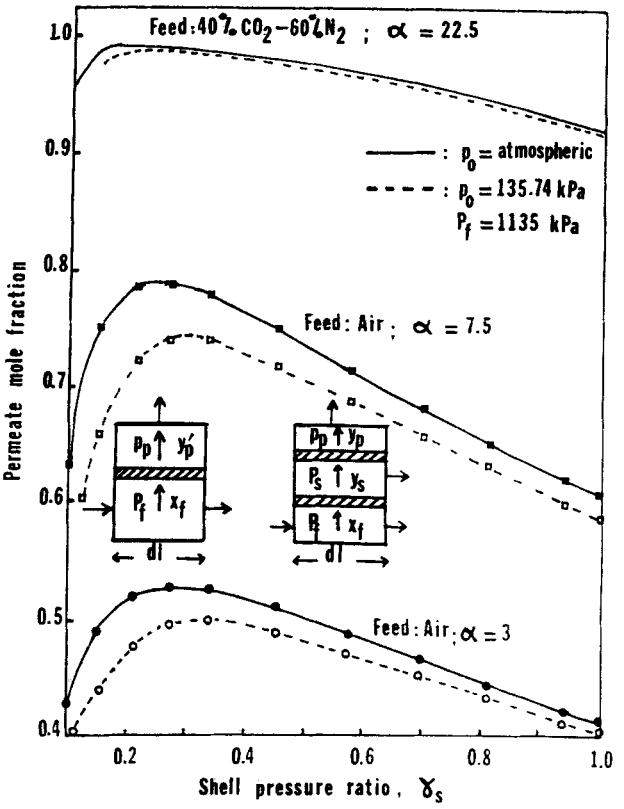

Figure 7. Two-step permeation analysis at zero stage cut: simulation only.

zero stage cut permeation are shown. Next, we present the experimental data from a hollow-fiber ISP and compare the results with those from our theoretical model. The above experimental data have also been compared with those from the same permeator operated as a conventional permeator. We have compared (numerically) the performance of the ISP with the corresponding two-stage cascade where each stage is a single hollow-fiber permeator. We then explore the effect of recycling the shell-side product stream to the feed gas on the final product quality and quantity. Finally, we have compared the ISP performance with a conventional permeator with recycle.

Figure 7 shows the final process permeate mole fraction y_p against the shell pressure ratio $\gamma_s = P_s/P_f$ for given P_f and p_p in a zero stage cut permeation process. Calculations were carried out for two values of p_p, atmospheric and 135.74 kPa, respectively. For feed air (O_2—N_2) with $x_f = 0.21$ and $P_f = 1{,}135$ kPa, two membrane selectivities were chosen, $\alpha = 3$ and 7.5. For a CO_2—N_2 feed with $x_f = 0.40$ and the same P_f, an α value of 22.5 was selected. Note that the performances for two extreme values of γ_s ($=1$ and $=\gamma'$) correspond to those of a conventional permeator.

Figure 7 illustrates how, without any expenditure of additional energy, the internally staged permeation yields a better quality permeate than a conventional permeator. Thus two-step permeation can produce a higher enrichment than a single-step permeation process. The extent of this extra enrichment is considerable. In particular, there is a value of γ_s where the extra enrichment is maximum. Such a behavior may be explained as follows.

The final process permeate y_p is a function of the first permeate composition y_s and the second stage pressure ratio γ_p. As the first stage pressure ratio γ_s increases, y_s decreases, lowering y_p. At the same time, however, γ_p decreases, which leads to a higher y_p. The increase in y_p due to a decrease in γ_p more than offsets initially the decrease in y_p due to a decrease in y_s from increasing γ_s. However, as γ_s keeps on increasing, the situation changes so that there is a maximum in y_p at a relatively low γ_s. Further, the maximum does depend on the value of p_p, α, and x_f.

We now focus on the ISP where the stage cut is nonzero. Before we present the data from the ISP, we provide the pure-component permeability information essential for modeling the ISP behavior. Note that permeability measurements were carried out *in situ* in the tube-side mode with the first set of fibers and in the shell-side mode with the other set of fibers. The species are O_2, N_2, and CO_2; their pure-component specific permeabilities at 21°C are shown in Figure 8.

This figure shows that for the pressure range studied, the specific permeabilities are essentially constant. Further, the specific permeabilities in the tube-side and shell-side modes are almost identical for O_2 and N_2. However, the tube-side data for CO_2 are somewhat higher than the shell-side data. This may be attributed to a few blocked fibers in the first set of CA fibers operated in the tube-side mode (the role of extra plasticization in this mode is unknown at this pressure level). This effect is not

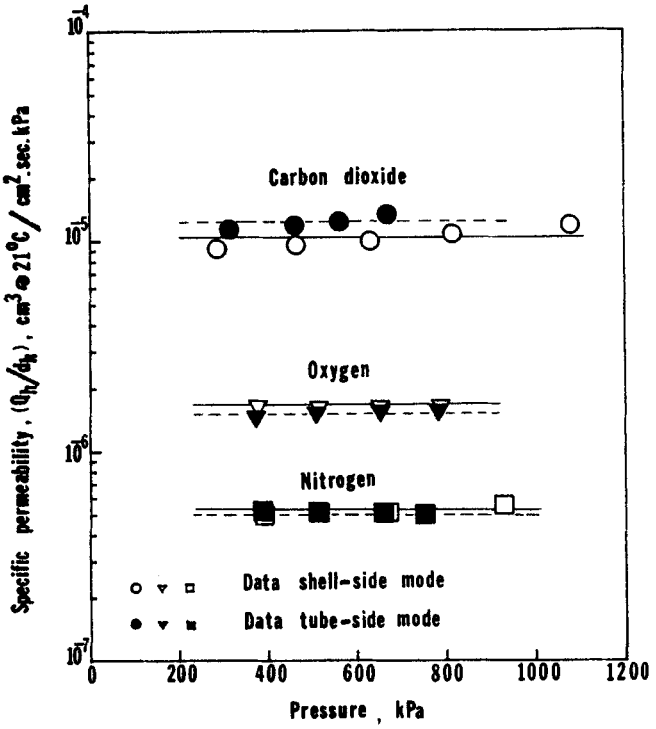

Figure 8. Pure component specific permeabilities.

visible in the data for O_2 and N_2 since their permeabilities are an order of magnitude lower than that of CO_2. In the simulation of the ISP behavior, therefore, all specific permeabilities were assumed independent of pressure. The experimental values of the tube-side mode and the shell-side mode were used in their respective simulations.

While Figure 7 dealt with model calculations for internally staged permeation under zero stage cut situation, we show in Figures 9 and 10 the experimental data from the ISP of this study for two binary feed gas mixtures of O_2—N_2 (air) and 40% CO_2–60% N_2, respectively. The feed mixture in each case was introduced to the lumen of the first set of fibers at 1,135 kPa. The shell-side pressure was maintained at 446 kPa and the shell-side flow was countercurrent to the high pressure feed. The final process permeate stream, countercurrent to the shell-side stream, exited from the lumen of the second set of hollow fibers at atmospheric pressure. These two figures also indicate the observed performances of the same hollow-fiber permeator operated countercurrently in the conventional mode: the feed gas mixture entered the shell side at 1,135 kPa and permeate was collected simultaneously from the lumen of both sets of fibers at atmospheric pressure.

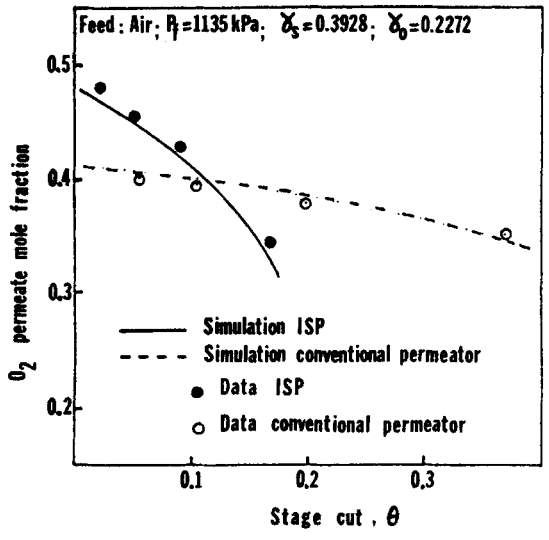

Figure 9. ISP vs. conventional permeator, countercurrent mode, feed: air.

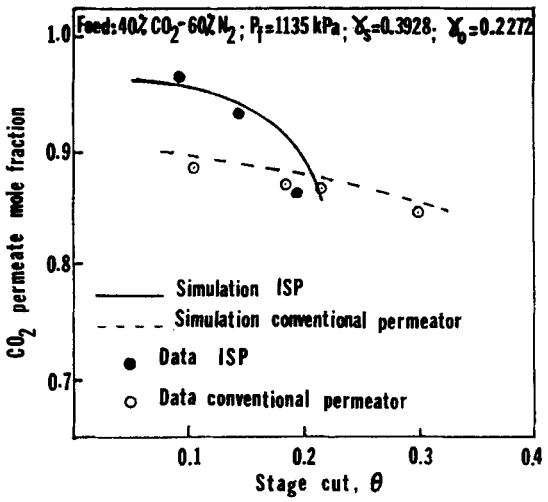

Figure 10. ISP vs. conventional permeator, countercurrent mode, feed: 40% CO_2–60% N_2.

Both figures demonstrate that at lower cuts the final process permeate quality from the ISP is much higher than that from the same permeator operated in the conventional mode. The extra enrichment is considerable. Both figures also show that this particular ISP is such that at high stage cuts, its performance deteriorates to a level lower than that of a conventional permeator. Thus, without any recycle or reflux, a hollow-fiber gas permeator, suitably configured as an ISP, can yield a permeate of higher quality than the maximum achievable in a conventional hollow-fiber permeator. For higher rates of production with a significantly lower permeate quality, the same permeator could easily be operated in the conventional mode.

The results of numerical simulations of the ISP and the conventional permeation modes are shown in Figures 9 and 10 as solid and dashed lines, respectively. It is obvious that the mathematical formulation based on the homogeneous membrane model predicts the ISP separation performances well. Note that the simulation includes pressure drop in the fiber lumen.

The reasons for a sharper drop in the process permeate quality at higher stage cuts in ISP are several: low value of the ratio N_2/N_1 in the particular permeator used and countercurrent flow. The effect of a cocurrent flow pattern in the ISP is studied in Figure 11 for a 40% CO_2–60% N_2 gas mixture, under pressure conditions identical to those of Figures 9 and 10. Specifically, the feed, shell, and permeate pressures were maintained at 1,135 kPa, 446 kPa, and atmospheric, respectively. First, the data agree quite well with the numerical results shown by the solid line. Second, the data show that the process permeate quality

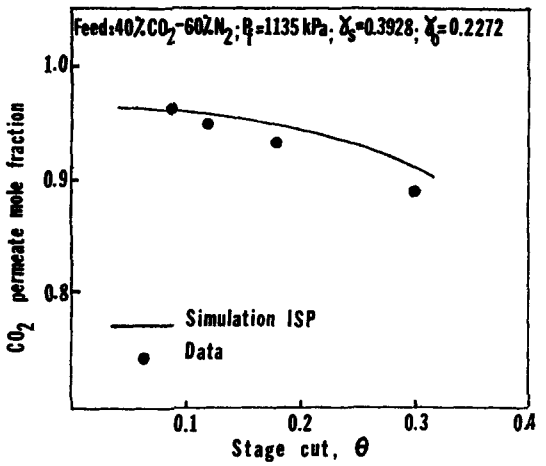

Figure 11. ISP in cocurrent mode.

decreases with the overall stage cut much more slowly than in Figure 10. This would indicate that for the conditions employed, the cocurrent flow pattern is superior to the countercurrent flow pattern in the ISP mode.

To check whether the simulation model predicts such a behavior, we have plotted the simulation results in Figure 12 for cocurrent and countercurrent flow with a 40% CO_2–60% N_2 feed gas for the same parametric conditions. The simulations clearly show that at high stage cuts the cocurrent pattern produces a higher permeate composition. This is in clear contrast to well-known results for a conventional permeator having a homogeneous membrane (Blaisdell and Kammermeyer, 1973), namely, countercurrent flow pattern leads to better separation. We seek now to explain the origin for such a contrary behavior in an ISP.

Consider Figure 13, where the CO_2 partial pressure profiles in the feed, shell, and permeate regions are plotted against the dimensionless membrane length in an ISP for cocurrent and countercurrent flow patterns. These profiles correspond to an inlet feed flow rate of 50 scc/min, and feed, shell, and process permeate outlet pressures of 1,135 kPa, 446 kPa, and atmospheric, respectively. It is obvious that the CO_2 partial pressures in two permeate regions (shell and process permeate) for the

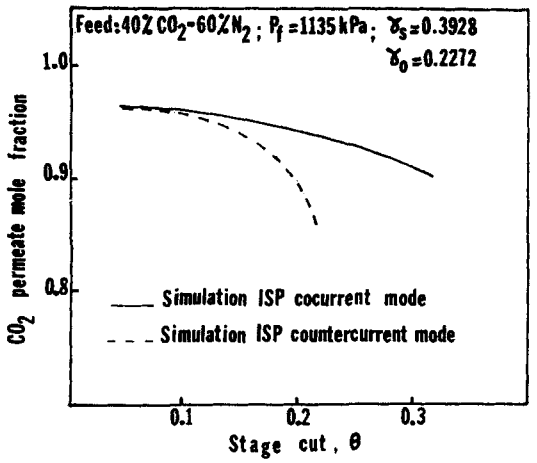

Figure 12. Effect of flow pattern in ISP.

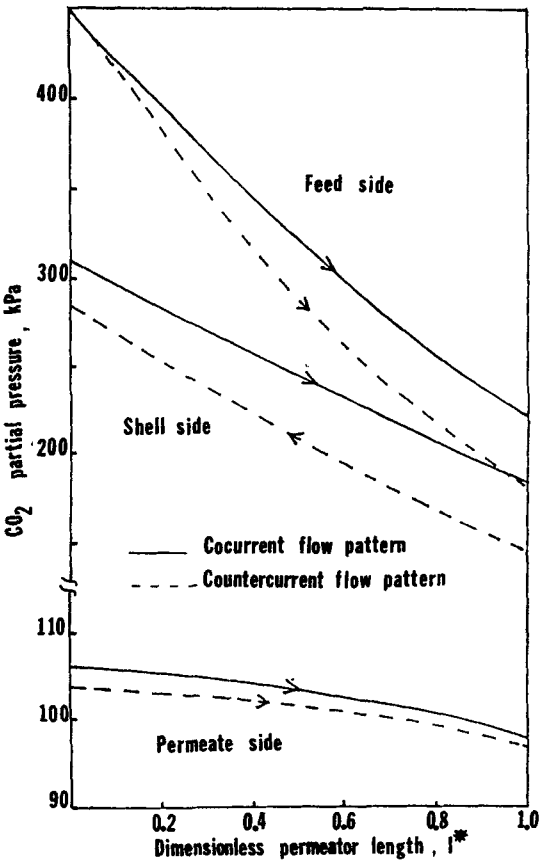

Figure 13. Comparison of CO_2 partial pressure profiles in cocurrent and countercurrent modes in ISP.

cocurrent mode are higher than those for the countercurrent mode. In particular, the local CO_2 partial pressure difference between the shell and the process permeate stream for concurrent flow is higher than that for the countercurrent flow all along the permeator length. This excess partial pressure difference translates directly into higher purification in the second stage.

The shell-side CO_2 partial pressure profile is crucial in this regard. Because of permeation through the second membrane, the shell-side CO_2 partial pressure in countercurrent flow cannot come up to the high value it normally attains at the permeate exit. On the other hand, the highest CO_2 partial pressure in the shell in cocurrent flow is unaffected by permeation through the second membrane. If the highest CO_2 partial pressure in the shell side may be loosely considered as a key trendsetter of process permeate quality, then the cocurrent mode clearly wins out. Obviously, as the stage cut decreases, the effect of permeation into the second stage decreases and the performances come closer to one another. It should be noted that the ISP could be operated in other modes, such as a combination of cocurrent and countercurrent flow, and that cocurrent flow is not necessarily the best mode of operation. However, in this paper we have considered only simple cocurrent and countercurrent modes of operation.

Next, we compare the performance of the ISP with the corresponding two-stage series configuration in Figure 3 for the same total membrane area. The following operational modes have been chosen for each system: cocurrent flow pattern for the ISP,

and countercurrent flow pattern for the series configuration. The simulation results for a 40% CO_2–60% N_2 feed gas are presented in Figure 14. The feed, shell, and permeate pressures were 1,135 kPa, 446 kPa, and atmospheric, respectively. Figure 14 shows that the ISP in concurrent mode yields a slightly better performance than the series configuration with countercurrent flow pattern. For a lower α system, this difference will be much higher (Sidhoum et al., 1988b). Note that for the series configuration, countercurrent flow was selected since it is the best mode of operation.

In an ISP, three process streams are obtained: a high-pressure reject stream depleted in the more permeable species, an enriched permeate stream, and a shell reject stream, whose composition lies between the feed inlet and permeate compositions. In order to increase the process permeate composition and amount, one may recycle partially or totally the shell reject stream to the feed inlet stream.

Recycling in membrane-based separation schemes to improve permeate quality has been studied with a conventional permeator (Kimura and Walmet, 1980; Heit, 1982; Teslik, 1983; Stern et al., 1984; Teslik and Sirkar, 1986; Majumdar et al., 1987). In these schemes, part of the permeate stream recycled to the feed inlet results in a loss of productivity. However, in the ISP there is no loss of productivity since the shell reject is recycled instead of the permeate. Further, the extra energy consumed in the ISP per unit process permeate product will at the most be 10%.

Simulation studies have been therefore carried out for a CO_2–N_2 system with feed, shell, and outlet permeate pressures of 1,135 kPa, 446 kPa, and atmospheric, respectively. The computed results are presented in Figure 15 for countercurrent flow. It is shown that as the fraction of the shell-side reject recycled is increased, the permeate composition increases at a given stage cut. Note also that at total recycle ($\eta = 1$), the CO_2 permeate mole fraction vs. stage cut curve becomes almost flat for a large stage cut range. Such behavior is highly desirable. It will also lead to higher productivity from the permeator in the ISP mode.

Finally, the performance of ISP without any recycle is compared with that of the conventional permeator with or without recycle. The comparison is based on net permeate productivity and power requirement for a fixed total membrane area. The

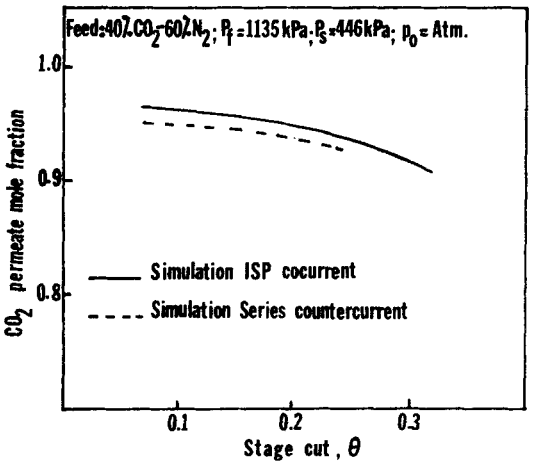

Figure 14. ISP in cocurrent mode vs. two-stage cascade in countercurrent mode.

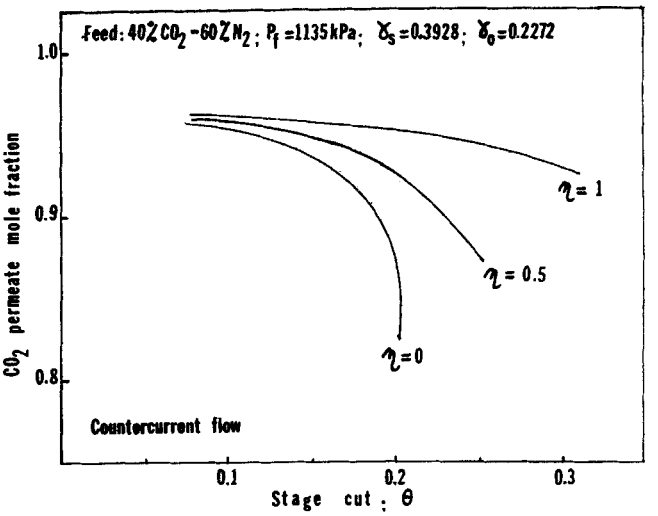

Figure 15. Effect of shell reject stream recycle in ISP.

simulated results are shown in Table 2 for the O_2–N_2 (air) system. The quantity η_1 represents the fraction of the permeate stream recycled to the feed inlet of the conventional permeator.

Table 2 shows, as expected, that for the no-recycle scheme the permeate flow rate output obtained with the conventional permeator is much higher than that achieved with the ISP. However, for the feed flow rate range studied (30 to 600 cm^3/min at 21°C) the conventional permeator leads to much lower permeate compositions in the more permeable species (O_2) compared to those obtained with the ISP.

Recycling part of the permeate, in the conventional permeator, increases the permeate composition at the expense of the permeate productivity, $(1 - \eta_1)V$, and is associated with a high power requirement. The additional compression power requirement in the recycle scheme is proportional to the quantity $\eta_1 V \ln (P_f/p_o)$ reported in Table 2, assuming isothermal compression. This table clearly illustrates the superiority of the ISP over the conventional permeator when high product quality is specified.

Conclusions

A novel membrane gas separation scheme identified as internally staged permeation has been proposed. This scheme is

Table 2. Comparison of ISP and Corresponding Conventional Permeator with and without Recycle for Air Separation: Simulation Results, Countercurrent Flow Pattern

			Conventional Permeator*				
ISP* $\eta = 0$			$\eta_1 = 0$		$\eta_1 = 0.9$		
L_f	V	y_p	V	y_p'	$(1 - \eta_1)V$	y_p'	PW
600	1.881	0.473	15.90	0.412	1.603	0.4197	34.86
400	1.884	0.475	15.89	0.410	1.606	0.4215	34.91
200	1.884	0.475	15.80	0.404	1.613	0.4267	35.09
100	1.876	0.471	15.63	0.392	1.629	0.4368	35.43
60	1.864	0.464	15.38	0.375	1.649	0.4492	35.85
40	1.846	0.454	15.08	0.353	1.671	0.4633	36.35
30	1.828	0.444	14.77	0.329	1.692	0.4757	36.80

*Both permeators have the same total membrane area; P_f = 1,135 kPa; P_s = 446 kPa; p_o = atmospheric; $PW = \eta_1 V \ln (P_f/p_o)$; L_f and V in cm^3/min, 21°C

based on a newly proposed two-step permeation scheme, as opposed to a one-step permeation scheme in conventional membrane gas separation. Two-step permeation produces a richer permeate without any additional energy expenditure.

It was demonstrated that the theoretical predictions based on the homogeneous membrane model fit very well the experimental performances of a hollow-fiber based ISP containing asymmetric cellulose acetate hollow fibers, for cocurrent as well as countercurrent flow patterns.

At low stage cuts the ISP easily outperforms the conventional permeator and produces a more enriched permeate at a given stage cut.

The ISP has a better composition vs. stage cut performance in cocurrent flow than in countercurrent flow for the conditions used in this study. This has been demonstrated experimentally and theoretically.

Numerical simulations have shown that the ISP in cocurrent mode performs better than the series configuration with countercurrent flow pattern.

One way to improve the performance of an ISP is to recycle the intermediate pressure shell reject stream to the feed stream. Theoretical calculations demonstrate that indeed it significantly improves the stage performance.

Since the ISP can easily be configured as a conventional permeator with shell-side feed, such a permeator can be used for two purposes. When an enrichment level higher than that achievable by a conventional permeator is required, the permeator should be configured as an ISP. For lower enrichment levels, the same permeation device should be operated as a conventional permeator.

Acknowledgment

M. Sidhoum was awarded the Presidential Scholarship at Stevens Institute of Technology while pursuing this study. The senior author acknowledges the financial support of the BOC group during 1987–1988.

Notation

D_i, D_o = inside, outside diameters of cellulose acetate hollow fibers
D_{lm} = log mean diameter, Eq. 14
K_1^I, K_1^{II} = constants, Eq. 14
K_2^I, K_2^{II} = constants, Eq. 17
l = distance
l_e = total effective length of permeation
l_p = potted length of cellulose acetate hollow fibers
l^* = dimensionless distance, Eq. 14
L = local feed flow rate
L_i = first stage permeate flow rate in two stage cascade
L_f = fresh feed flow rate to permeator
L_{f1} = feed flow rate at permeator entry, applicable to recycle permeator
L_{R1} = high-pressure reject flow rate
L_{R2} = shell reject flow rate in ISP or second stage reject flow rate in two-stage cascade
L^* = dimensionless local feed flow rate, Eq. 14
L_{f1}^* = normalized value of L_{f1}, Eq. 7b
L_{R2}^* = normalized value of L_{R2}, Eq. 7b
N_1 = total number of CA hollow fibers in first stage
N_2 = total number of CA hollow fibers in second stage
p_o = process permeate outlet pressure
p_p = local process permeate pressure
P = local feed pressure
P_f = feed inlet pressure
P_s = shell pressure in ISP or in second stage of a two-stage cascade
Q_i = permeability of species i through homogeneous membrane
$(Q/d)_i$ = specific permeability of species i through CA fibers
R_g = universal gas constant
T = absolute temperature
V = local permeate flow rate in conventional single stage or two-stage permeation
V_p = local permeate flow rate in ISP
V_{pT} = total permeate flow rate in ISP or in two-stage cascade
V_s = local shell-side flow rate in ISP
V_p^* = normalized value of V_p, Eq. 14
V_{pT}^* = normalized value of V_{pT}, V_{pT}/L_f
V_s^* = normalized value of V_s, Eq. 14
x = local mole fraction of more permeable component in feed-side gas mixture
x_i = mole fraction of more permeable component in first stage permeate stream of two-stage cascade
x_f = mole fraction of more permeable component in fresh feed
x_{f1} = mole fraction of more permeable component at permeator entry, applicable to recycle permeator
x_{R1} = mole fraction of more permeable component in high-pressure reject stream
x_{R2} = mole fraction of more premeable component in shell reject stream of ISP or in second stage reject stream of two-stage cascade
y = local mole fraction of more premeable component in permeate side of conventional permeator
y_p = local mole fraction of more permeable component in permeate side of ISP
y_p' = permeate mole fraction of more permeable species in one-step permeation process
y_s = local mole fraction of more permeable component in shell-side stream of ISP

Greek letters

α = ideal separation factor, Eq. 1b
γ = pressure ratio, Eq. 14
γ_1 = value of γ at $\ell^* = 1$
γ_s = pressure ratio, Eq. 1b
γ_p = pressure ratio, Eq. 3b
γ_o = permeate pressure ratio, $= p_o/P_s$
γ' = pressure ratio, Eq. 5b
η = fraction of shell reject stream recycled to feed inlet stream of ISP
η_1 = fraction of permeate stream recycled to feed inlet stream in conventional permeator
θ = overall stage cut, (process permeate flow rate/fresh feed flow rate)
μ = gas mixture viscosity

Literature Cited

Blaisdell, C. T., and K. Kammermeyer, "Countercurrent and Cocurrent Gas Separation," *Chem. Eng. Sci.*, **28**, 1249 (1973).

Heit, L. B., "An Experimental Investigation of a Light Fraction Recycle Permeator for Oxygen-Enrichment," M. Eng. Thesis, Dept. Chemistry and Chem. Eng., Stevens Inst. Technol., Hoboken, NJ (1982).

Kao, Y. K., S. Chen, and S. T. Hwang, "Effect of Diffusion on the Model of a Capillary Gas Permeator," *J. Membrane Sci.*, **32**, 139 (1987).

Kimura, S. G., and G. E. Walmet, "Fuel Gas Purification with Permselective Membranes," *Sep. Sci. Technol.*, **15**, 1115 (1980).

MacDonald, W., and C. Y. Pan, "Method for Drying Water-Wet Membranes," U.S. Pat. No. 3,842,515 (1974).

Majumdar, S., L. B. Heit, A. Sengupta, and K. K. Sirkar, "An Experimental Investigation of Oxygen-Enrichment in a Silicone Capillary Permeator with Permeate Recycle," *Ind. Eng. Chem. Res.*, **26**, 1434 (1987).

Ohno, M., O. Ozaki, H. Sato, S. Kimura, and T. Miyauchi, "Radioactive Rare Gas Separation Using a Separation Cell with Two Kinds of Membrane Differing in Gas Permeability Tendency," *J Nuclear Sci. Technol.*, **14**, 589 (1977).

Pan, C. Y., and H. W. Habgood, "An Analysis of the Single-Stage Gas-

eous Permeation Process," *Ind. Eng. Chem. Fundam.*, **13,** 323 (1974).
Perrin, J. E., and S. A. Stern, "Modeling of Permeators with Two Different Types of Membranes," *AIChE J.*, **31,** 1167 (1985)
———, "Separation of a Helium-Methane Mixture in Permeators with Two Different Types of Polymer Membranes," *AIChE J.*, **32,** 1889 (1986).
Sengupta, A., "Investigations on Binary and Ternary Gas Separations Using Polymeric Membrane Permeators," Ph.D. Diss., Dept. Chemistry and Chem. Eng., Stevens Inst. Technol., Hoboken, NJ (1985).
Sengupta, A., and K. K. Sirkar, "Multicomponent Gas Separation by an Asymmetric Permeator Containing Two Different Membranes," *J. Membrane Sci.*, **21,** 73 (1984).
———, "Ternary Gas Mixture Separation in Two-Membrane Permeators," *AIChE J.*, **33,** 529 (1987).
———, "Ternary Gas Separation Using Two Different Membranes," *J. Membrane Sci.*, **39,** 61 (1988).
Sidhoum, M., "Gas Separation with Asymmetric CA Hollow Fibers: Models, Experimental Behavior, and New Separation Concepts," Ph.D. Diss., Dept. Chemistry and Chem. Eng., Stevens Inst. Technol., Hoboken, NJ (1988).
Sidhoum, M., A. Sengupta, and K. K. Sirkar, "Asymmetric Cellulose Acetate Hollow Fibers: Studies in Gas Permeation," *AIChE J.*, **34,** 417 (1988a).
Sidhoum, M., S. Majumdar, R. R. Bhave, A. Sengupta, and K. K. Sirkar, "Experimental Behavior of Asymmetric CA Membranes and Its Use in Novel Separation Schemes," *New Membrane Materials and Processes for Separation,* K. K. Sirkar, D. R. Lloyd, eds., *AIChE Symp. Ser.*, **84**(261), 102 (1988b).
Sirkar, K. K., "Separation of Gaseous Mixtures with Asymmetric Dense Polymeric Membranes," *Chem. Eng. Sci.*, **32,** 1137 (1977).
Stern, S. A., J. E. Perrin, and E. J. Naimon, "Recycle and Multimembrane Permeators for Gas Separations," *J. Memb. Sci.*, **20,** 25 (1984).
Teslik, S., "Analysis of a Light Fraction Recycle Permeator and Oxygen Enrichment Separation Schemes," M. Eng. Thesis, Dept. Chemistry and Chem. Eng., Stevens Inst. Technol., Hoboken, NJ (1983).
Teslik, S. and K. K. Sirkar, "A Comparative Analysis of the Role of Recycle or Reflux in Permeators Separating a Binary Gas Mixture," *Recent Developments in Separation Science,* **9,** N. N. Li, J. M. Calo, eds., CRC Press, OH, 245 (1986).
Walawender, W. P., and S. A. Stern, "Analysis of Membrane Separation Parameters. II: Countercurrent and Cocurrent Flow in a Single Permeation Stage," *Separ. Sci.*, **7,** 553 (1972).

Manuscript received July 5, 1988, and revision received Jan. 30, 1989.